LOW-TEMPERATURE SOLDERING FOR THE INTERCONNECTION OF SILICON HETEROJUNCTION SOLAR CELLS

Angela De Rose*, Denis Erath, Torsten Geipel, Achim Kraft, and Ulrich Eitner
Fraunhofer Institute for Solar Energy Systems ISE, Heidenhofstraße 2, 79110 Freiburg, Germany
*Phone: +49 (0)761 4588 5856, angela.de.rose@ise.fraunhofer.de

ABSTRACT: Interconnecting silicon heterojunction (SHJ) solar cells by low-temperature ribbon soldering allows the use of standard stringing equipment and might therefore be the cheapest and most straightforward implementation in existing fabrication lines. However, solder joints on low-temperature metallization pastes of SHJ cells are known for a weak adhesion to the cell surface. This work is dedicated to a better understanding of the interaction between solder and low-temperature metallization on SHJ solar cells. We evaluate soldering during a lamination process with standard copper ribbons featuring six different low-temperature solder alloys. The mechanical adhesion of the solder joints and microstructural changes in the metallization pastes during the soldering process are analyzed. Our study includes three metallization pastes, two of them show poor adhesion on the wafer surface after soldering (up to 0.03 N/mm) and one paste performs slightly better (up to 0.28 N/mm). We find this difference to be caused by an interaction of the pastes and the liquid solder, neither depending on the composition of the solder alloy nor on the soldering time. A fine grain structure of the Ag-particles of such pastes correlates with a higher penetration of solder components (Sn and Bi) resulting in dissolution of the metallization and detachment from the cell surface.
Keywords: Interconnection, Heterojunction, Soldering, Low-temperature

1 INTRODUCTION

Crystalline silicon solar cells based on heterojunction technology are one of the most promising concepts to obtain very high energy conversion efficiencies. The world record efficiencies reached within the last years underline the competitiveness of this technology [1–3]. Recently, Yoshikawa *et al.* presented a record cell efficiency above 26% combining heterojunction and back-contact technology [4]. A lean production chain with low-temperature processes and carrier selective hetero-structure for excellent passivation are main advantages of silicon heterojunction (SHJ) solar cells. Due to their higher open circuit voltage and their lower temperature coefficient of power, they offer a superior module performance compared to homojunction cells.

Consequently, an industrially feasible interconnection process in photovoltaic module fabrication becomes important. Recent activities address the use of alternative and non-standard interconnection approaches like electrically conductive adhesives [5] or wire interconnection [6]. To ensure an easy and cost-efficient implementation with conventional stringers, our work focuses on an interconnection by ribbon soldering with lead-free low-temperature solder alloys.

Since the passivation by the amorphous silicon layers of SHJ cells cannot withstand temperatures above 250 °C [7, 8], low-temperature soldering is considered as a suitable technology. The main challenge is to overcome the known weak adhesion between metallization paste and wafer surface, observed after soldering on SHJ solar cells [9].

Bismuth-based solder alloys possess lower melting points than common tin-lead-based solders and can therefore be processed at temperatures below 200°C. The approach followed in this work is to interconnect three commercially available low-temperature metallization pastes for SHJ solar cells with copper ribbons featuring six different solder coatings by soldering and examine the interaction between the materials. We analyze the differences and show relations between mechanical, optical and microstructural properties of the three pastes under investigation.

2 EXPERIMENTAL

2.1 Sample fabrication

The experimental procedure including sample fabrication (green) and characterization techniques (orange) is depicted in Figure 1. Our experiments are performed with bifacial monocrystalline SHJ solar cells (156×156 mm^2) from Meyer Burger Technology AG. The cells are industrially pre-processed on n-type Cz-Si 6'' wafers with a-Si:H(i)/a-Si:H(n+)/TCO on the front side and a-Si:H(i)/a-Si:H(p+)/TCO on the rear side [10]. Based on previous investigations focusing on screen printing quality [11], the busbars at the front and rear side are prepared in a five-busbar design with three different metallization pastes "A" to "C" (Ag content between 85 - 95%; different amount of solids). The pastes are cured for t_{cur} = 4.5 min at T_{cur} = 200 °C in an inline infrared/convection furnace after each screen printing step on the front and rear side.
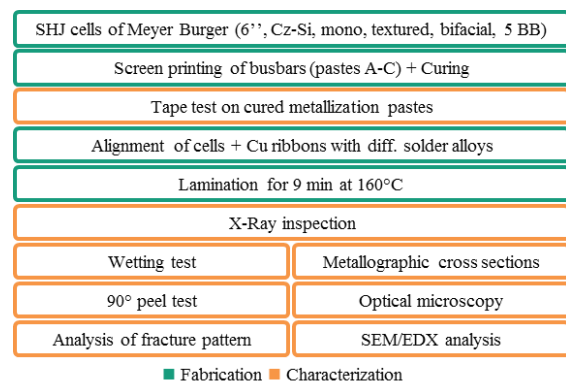

Figure 1: Schematic process sequence for fabrication and characterization of low-temperature soldered joints on SHJ solar cells.

A set of samples is fabricated for mechanical peel tests and for preparation of cross sections, respectively. Our analysis includes bare and solder-coated copper ribbons (1.5 mm × 0.18 mm) with six bismuth-based solders and a tin-lead solder as reference, see in Table I.

Table I: Overview on composition, melting point and delivery of the processed solder alloys.

	Composition (wt. %)	Melting Point (°C)	Form
SnBi	43/57	139	coating
	60/40	139 - 150	coating
	42/58	139 - 140	paste
SnBiAg	41/57/2	138 - 142	coating
	60/38/2	153 - 156	coating
PbSnBi	42/37/21	118 - 122	paste
SnPb	60/40	183 - 187	coating

The solder pastes are manually stencil printed onto the cell and covered with bare copper ribbons, whereas the ribbons with solder coating are attached to the busbars without additional solder paste. The melting point of the bismuth alloys allows the use of a lamination process step ($t_{lam} \approx 9$ min, $T_{lam} = 160$ °C) for interconnection and therefore a process simplification. As reference, SnBi 43/57 and SnPb 60/40 coated ribbons are soldered manually onto the metallization of SHJ cells for comparison to shorter soldering times ($t_{man} \approx 1 - 2$ s, $T_{man} = 160 - 220$ °C).

2.2 Characterization of solder joints

The fabricated samples are characterized by X-ray inspection, wettability analysis, peel tests and microscope as well as SEM/EDX images at prepared cross sections. Prior to the solder joint analysis, tape tests on the metallization pastes (after curing) are performed to qualify the initial adhesion (before soldering) on the wafer. An adhesive tape is pulled off in an angle of 90° from the pastes whereas the force is detected.

X-ray inspection as a non-destructive method is well suited to provide an insight into the quality of the solder joints [12]. Voids, caused by air trapped within the joint, reduce the contact area and thus result in a higher electrical resistance and lower adhesion strength. They can be detected by a difference in contrast within the X-ray image.

Prior to soldering, the wettability of the screen printed and cured low temperature metallization with the liquid solder alloys is analyzed. The cells are placed on a hotplate and pre-heated to 200 - 220 °C so that the solder melts as soon as it comes in contact with the metallization. A flat shiny appearance of the solder (low contact angle) indicates good wettability whereas solder drops (high contact angle) are referred to de-wetting.

The mechanical strength of the interconnection is characterized by peel tests according to DIN EN 50461, requiring forces larger than 1 N/mm [13]. The adhesion force of the soldered ribbon is recorded against the position along the busbar. The ribbons are peeled off in an angle of 90° to the cell surface with a speed of 50 mm/min. The resulting fracture pattern gives information about the weakest interface. We distinguish between an adhesive fracture where the metallization is separated from the solar cell, and a cohesive fracture within the metallization paste.

In order to inspect the cross section of the solder joints, a part of the soldered busbar is cut by a precision saw, embedded into a nickel-containing epoxy, ground and polished. Optical microscopy is used to inspect the formation of the solder joints.

Scanning electron microscopy (SEM, Carl Zeiss Microscopy Auriga 60) is performed on a crossbeam workstation in combination with energy diffractive X-ray (EDX, Bruker Quantax XFlash 6│60 detector) spectroscopy. Both methods reveal information on the cross section of the solder joint, especially on intermetallic phase formation [14].

3 RESULTS AND DISCUSSION

3.1 Wetting and mechanical adhesion

Based on the knowledge of a weak adhesion between metallization and solar cell after curing but before soldering [9], tape tests along the metallization of all three pastes are carried out in pretests. The measured average normalized peel forces exceed values above 0.9 N/mm for all pastes, limited by the adhesion of the tape on the paste (see Figure 2 (a)). These values are considered high enough for a successful interconnection.
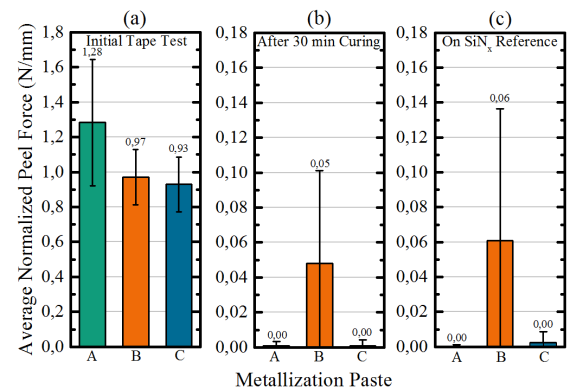

Figure 2: Experimental results of 90° tape test on the initial pastes after curing for 4.5 min (a) and of 90° peel test after soldering with SnBiAg 41/57/2 (b, c) as a function of metallization paste (A - C). Each box contains data of two peel tests, showing average and standard deviation. Note the different scaling of (b) and (c) compared to (a).

A set of the aforementioned SHJ solar cells is employed to test the wetting behavior of the metallization pastes and to investigate the mechanical adhesion after soldering (see left column (orange) of process sequence in Figure 1). All three pastes show good wettability for the used solder alloys which is the requirement for a successful solder process. The results of the mechanical peel tests, including each the data for one ribbon peeled off, are shown in Figure 3. Average and standard deviation of the normalized peel force are plotted as a function of metallization paste (A - C) and solder alloy (green: ribbon coatings, blue: solder pastes, grey: ribbon coatings soldered manually). In agreement to previous investigations by Gierth *et al.* [9], all combinations show poor adhesion. Paste B yields considerably higher values with 0.21 N/mm and 0.28 N/mm when using PbSnBi 42/37/21 and SnBi 43/57, respectively. We exclude the contact area of the solder joint to be the reason for this prominent deviation between pastes A - C due to homogenous solder joint formation proven by X-ray imaging. Exemplarily, the X-ray images for SnBiAg 60/38/2 on paste A, B and C are given in the inset of Figure 3, showing homogeneous solder joints along the busbar. The formation of those solder joints without any voids seems to be supported by the vacuum (~ 1 mbar) during the lamination process.

Figure 4 presents the force-path diagram for SnBi 43/57 on paste A (orange), on paste B (green) and for SnPb 60/40 soldered manually onto paste B (grey). The adhesion on paste B is higher along the whole length of the metallization. The fracture patterns (top-view microscopy images of busbars after peel test), also given in Figure 4, reveal a mostly cohesive fracture within the metallization for paste B. For paste A and paste C, the fracture is identified to be an adhesion failure between metallization paste and cell surface (TCO), which correlates with the measured adhesion. This indicates that the interface of paste A and C to the TCO is the weakest interface in this material combination, independent from the used solder alloys.
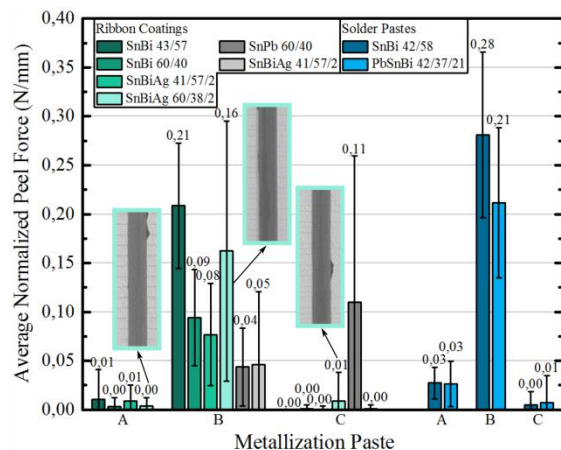

Figure 3: Experimental results of 90° peel test as a function of metallization paste (A - C) and solder alloy (color code). Four of the alloys are used as ribbons (green) and two are applied as solder pastes (blue), both processed during lamination for 9 min at 160 °C. As reference, two additional alloys are soldered manually (grey). Each data set gives average and standard deviation over one ribbon peeled off. In the inset, three X-ray images for SnBiAg 60/38/2 are shown exemplarily for a void-free solder joint formation.

In contrast to low-temperature pastes, the mechanical adhesion to the wafer for common high-temperature screen printing pastes is achieved by a firing step performed at temperatures up to 850°C. The contact formation is related to Ag-crystallites grown into the emitter thus ensuring electrical current path and mechanical stability [15]. Our pastes are dried within a short curing step for $t_{cur} = 4.5$ min at $T_{cur} = 220$ °C which leads to evaporation of solvents and to sintering of the Ag-particles. These effects differ fundamentally from the implications of the firing step. To improve the mechanical adhesion of paste A and C within our possibilities, a variation of the curing time up to 30 min is done [11], yielding no effect on wetting behavior or mechanical adhesion after soldering. Figure 2 (b) shows the corresponding peel test data with better results for paste B. As a reference measurement, homojunction solar cells with an anti-reflection coating (SiN_x) on the front side are processed and screen printed with the investigated metallization pastes A - C. Soldering and peel tests are performed in the described procedure. Most of the fracture patterns are also adhesive between paste and wafer resulting in zero adhesion (see Figure 2 (c)).

Consistently to the peel tests on TCO, paste B performs best with 0.06 N/mm, which suggests the TCO on the SHJ cells not to be the reason for the poor adhesion.
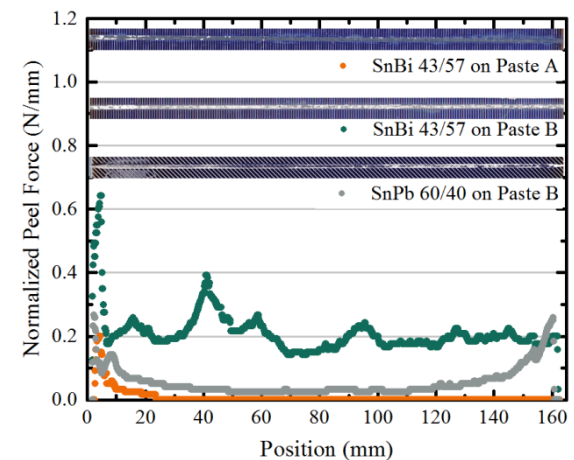

Figure 4: Normalized peel force of 90° peel tests plotted against the position along the busbar metallization. The graph includes the data for a ribbon coated with SnBi 43/57 on paste A (orange) and paste B (green) and as reference SnPb 60/40 on paste B (grey, soldered manually). The corresponding fracture patterns are shown above.

The fact that the initial adhesion is much higher than after soldering (see Figure 2 (a)) leads to the assumption that the loss in adhesion is induced by the liquid solder. This is confirmed by the performed wetting tests, exemplarily shown for a Bi- and a Pb-based solder alloy given in Figure 5. The application of the liquid solders onto metallization paste A leads to spalling from the cell surface in both cases, whereas paste B remains visually unaffected. Due to the fact that the TCO is not wettable, the liquid solder deforms. We conclude a fast reaction of paste A with the liquid solder which is supported by results from manually soldered solar cells where short soldering times of $1 - 2$ s are used. The Pb as well as the Bi references (grey in Figure 3 and Figure 4) show similar results which underlines that the loss of adhesion is caused within seconds after the contact with liquid solder, not depending on the composition of the solder alloy. The root cause of better adhesion of paste B may be found in the microstructure, wherefore cross sections of the solder joints are of great interest.
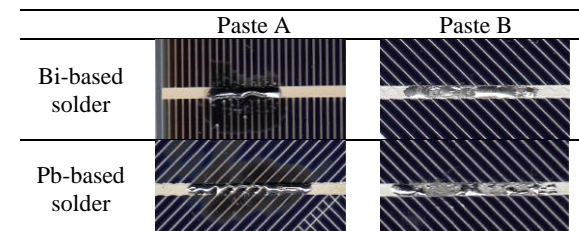

Figure 5: Wetting test with Bi- and Pb-based solder alloys on metallization paste A and B. Directly after contacting paste A with the liquid solder, the paste is spalling from the cell surface in contrast to paste B.
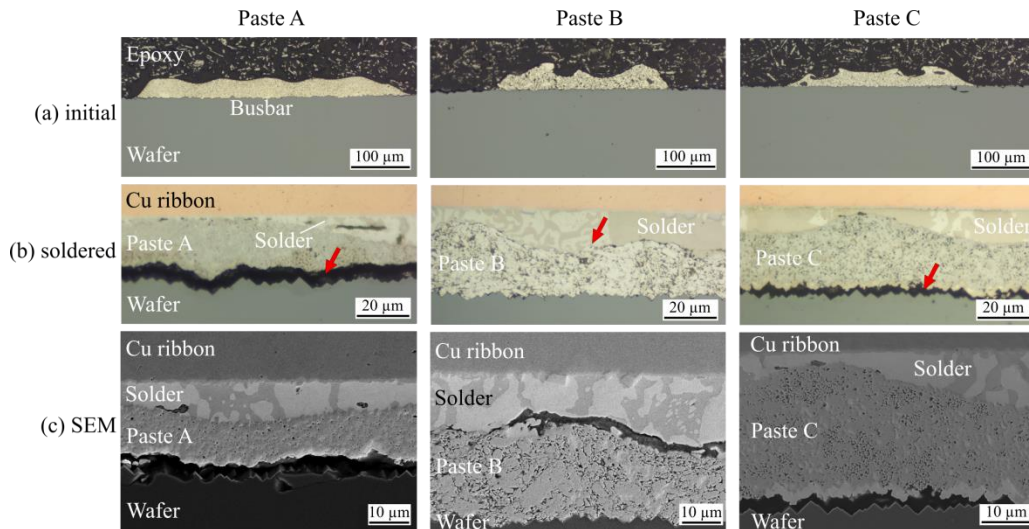
Figure 6: Optical microscopy images of metallographic cross sections of an unsoldered SHJ cell (a) and contacted with copper ribbons coated with SnBi 43/57 (b) on paste A, B and C. The red arrows mark the position of the gap after soldering. (c) Detailed SEM images of the cross sections shown above.

3.2 Microstructural characterization

Metallographic cross sections reveal a very small section of the entire soldered busbar and should therefore be interpreted carefully. Figure 6 (a) shows optical microscopy images with cross sections of bifacial SHJ cells in the uncontacted state. All pastes are initially in direct contact with the textured wafer surface which is in agreement with the good initial adhesion. The width of the busbars differs because of a tapered busbar design.

The metallization on the rear side is contacted with SnBi 43/57 coated copper ribbons and soldered during lamination (see Figure 6 (b)). The cross sections clearly reveal a gap between paste A and C and the wafer surface correlating with zero adhesion measured by the peel test. In case of paste B, the solder is in direct contact with the paste, as well as the paste with the wafer surface. Additionally, paste B features a coarser grain structure compared to paste A and C which is also confirmed by top view microscopy images (not shown here).

To focus in detail on the microstructure at those three interconnections, SEM is performed with higher magnification at the relevant interfaces (Figure 6 (c)). The difference in grain structure of Paste A and C compared to Paste B is clearly visible. Paste A and C appear finely grained and homogeneous whereas Paste B is relatively coarsely structured. The interfaces between paste A and C and solder do not show any cracking.

In contrast, paste B features larger and non-uniform grains and partially a gap between solder and paste. This SEM image shows a different position than given in Figure 6 (b) for paste B. Microscopy images with minor magnification reveal that the gap between paste B and solder appears only in parts. These differences in grain structure and the existence of the gap are suspected to influence the mechanical adhesion.

This idea is supported by energy dispersive X-ray (EDX) spectroscopy performed on the above shown cross sections. The results for paste B and C are given in Figure 7. EDX-mapping of the solder joints reveals a penetration of Sn (green) into the busbar which consists mainly of Ag (red). The Sn-penetration is more homogeneous and distinct for paste C (Figure 7 (b)), as well for paste A (not shown here). The finer grain structure of paste A and C seems to assist infiltration of liquid solder into the metallization paste because of an accompanying higher penetrability. An EDX element scan supports the assumption of an Ag_3Sn-phase formation at the solder-metallization-interface penetrating into the entire metallization. The growth of intermetallic compounds in solder joints on high-temperature metallization has already been studied in literature [14, 16] and depends strongly on temperature and exposure time. We exclude the time to be the relevant parameter due to similar results for the manually
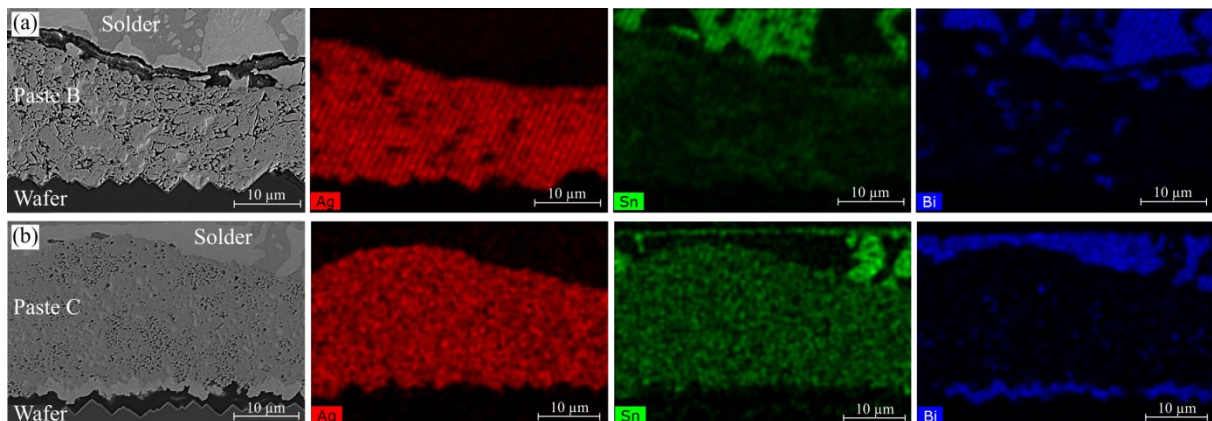

Figure 7: EDX element mapping of SnBi 43/57 solder joints on (a) paste B and (b) paste C.

soldered joints, as already assumed above. For paste B, the interaction with the liquid solder is found to be different. Beside the comparably low Sn-penetration, Bi (blue in Figure 7) seems to form clusters within the Ag-metallization. The occurring structure of Bi-phases is completely different for paste C. Bi agglomerates at the interface to the wafer and forms a solid Bi-layer. Compared to Sn or Pb, Bi is brittle [17] and shows a negative thermal expansion when melted and expands when solidified [14, 17–19]. The latter characteristic supports the ablation of the metallization from the cell surface. This finding is consolidated by the fracture pattern which is adhesive for paste C and cohesive when Bi is enclosed within the metallization (paste B).

The interaction of liquid solder and metallization paste strongly changes the structure of the metallization. Short soldering times are sufficient to induce an almost complete dissolution of the metallization and detachment from the cell surface. Intermetallic phase formation as well as Bi agglomeration at the wafer interface is found, which contribute to the embrittlement of the joint and ablation of the metallization.

4 CONCLUSION AND OUTLOOK

Peel tests on SHJ cells with six solder alloys on three different low-temperature metallization pastes reveal weak adhesion forces between cell surface and metallization after low-temperature soldering. Reference measurements using tape tests on unsoldered busbars prove that the loss in adhesion is caused by the solder diffusion. We show a relation between the mechanical adhesion of the pastes on the wafer after soldering, the grain structure of the pastes and penetration of Sn and Bi into the metallization. Paste B, which shows slightly higher peel forces, features a coarser grain structure which seems to impede the Bi penetration towards the wafer surface. Here, the fracture pattern after peel test shows a cohesive fracture within the paste, whereas an adhesive fracture is observed for two pastes with nearly zero adhesion. An interaction between liquid solder and paste occurs within the first seconds during soldering and leads to dissolving of the paste.

To realize the successful interconnection of SHJ solar cells with low-temperature soldering, an adaptation of the metallization pastes is indispensable. The penetration of liquid solder into the busbar should be reduced. Our results indicate that for instance a coarser grain structure may be beneficial.

5 ACKNOWLEDGEMENT

6 REFERENCES

[1] K. Masuko *et al.,* "Achievement of More Than 25% Conversion Efficiency With Crystalline Silicon Heterojunction Solar Cell," *IEEE J. Photovoltaics*, vol. 4, no. 6, pp. 1433–1435, 2014.

[2] M. A. Green *et al.,* "Solar cell efficiency tables (version 48)," *Prog. Photovolt: Res. Appl.*, vol. 24, no. 7, pp. 905–913, 2016.

[3] D. Adachi, J. L. Hernández, and K. Yamamoto, "Impact of carrier recombination on fill factor for large area heterojunction crystalline silicon solar cell with 25.1% efficiency," *Appl. Phys. Lett.*, vol. 107, no. 23, p. 233506, 2015.

[4] K. Yoshikawa *et al.,* "Silicon heterojunction solar cell with interdigitated back contacts for a photoconversion efficiency over 26%," *Nat. Energy*, vol. 2, no. 5, p. 17032, 2017.

[5] M. Späth *et al.,* "Hetero-junction module technology," in *Proceedings of the 26th European Photovoltaic Solar Energy Conference and Exhibition*, 2011, pp. 3121–3124.

[6] P. Papet *et al.,* "New Cell Metallization Patterns for Heterojunction Solar Cells Interconnected by the Smart Wire Connection Technology," *Proceedings of the Fifth Workshop on Metallization for Crystalline Silicon Solar Cells*, vol. 67, pp. 203–209, 2015.

[7] B. A. Korevaar *et al.,* "Influence of annealing on performance for hetero-junction a-Si/c-Si devices," in *Proceedings of the 23rd European Photovoltaic Solar Energy Conference and Exhibition*, 2008.

[8] S. de Wolf and M. Kondo, "Nature of doped a-Si: H/c-Si interface recombination," *Journal of Applied Physics*, vol. 105, no. 10, p. 103707, 2009.

[9] P. Gierth *et al.,* "Comparison of NiV and Polymer Paste Metallization as Low Temperature Interconnection of High Efficiency Heterojunction Solar Cells," in *Proceedings of the 28th European Photovoltaic Solar Energy Conference and Exhibition*, 2013, pp. 464–467.

[10] B. Strahm, "Heterojunction Solar Cells," Talk at nPV Workshop, Meyer Burger Research AG, 2017.

[11] D. Erath *et al.,* "Comparison of innovative metallization approaches for silicon heterojunction solar cells," *Silicon PV*, 2017, tbp.

[12] B. G. Batchelor, *Machine Vision Handbook,* 2nd ed.: Springer London Dordrecht Heidelberg New York, 2012.

[13] Solar cells - Datasheet information and product data for crystalline silicon solar cells, EN 50461: 2007-03, 2007.

[14] T. Geipel *et al.,* "Intermetallic compounds in solar cell interconnections: Microstructure and growth kinetics," *Solar Energy Materials and Solar Cells*, vol. 159, pp. 370–388, 2017.

[15] M. Hoerteis, "Fine-line printed contacts on crystalline silicon solar cells," PhD thesis, University of Konstanz, Germany, 2009.

[16] T. Geipel *et al.,* "Comprehensive study of intermetallic compounds in solar cell interconnections including lead-free, low melting point solders," in *Proceedings of the 32nd European Photovoltaic Solar Energy Conference and Exhibition*, 2016, pp. 479–486.

[17] H. H. Manko, *Solders and Soldering,* 3rd ed. New York, NY: S&P Global, 1992.

[18] M. J. Burek *et al.,* "Grain boundary effects on the mechanical properties of bismuth nanostructures," *Acta Materialia*, vol. 59, no. 11, pp. 4709–4718, 2011.

[19] Z. Mei and J. Morris, "Characterization of eutectic Sn-Bi solder joints," *JEM*, vol. 21, no. 6, pp. 599–607, 1992.